WATER RESERVOIRS MONITORING THROUGH GOOGLE EARTH ENGINE: APPLICATION TO SENTINEL AND LANDSAT IMAGERY

F. Bocchino [1,*], R. Ravanelli [1], V. Belloni [1], P. Mazzucchelli [2], M. Crespi [1,3]

[1] Geodesy and Geomatics Division, DICEA, Sapienza University of Rome, Rome, Italy
<filippo.bocchino, roberta.ravanelli, valeria.belloni, mattia.crespi>@uniroma1.it
[2] Aresys S.r.l., Italy – paolo.mazzucchelli@aresys.it
[3] Sapienza School for Advanced Studies, Sapienza University of Rome, Rome, Italy

KEY WORDS: Water reservoir monitoring, Sustainable Development Goals, Google Earth Engine, Sentinel, Landsat.

ABSTRACT:

Water reservoirs are subjected to increasing hydrological stresses, therefore continuous and accurate monitoring of these resources is essential to ensure their sustainable management. This work proposes a methodology to remotely monitor the surface extent of water reservoirs through the analysis of satellite multispectral and Synthetic Aperture Radar (SAR) images. In particular, a segmentation strategy was implemented within Google Earth Engine (GEE) to distinguish water bodies from the surrounding land surface and measure their extension, by applying three different approaches to Sentinel-1, Sentinel-2, and Landsat-8 imagery. The first approach is based on the use of the Automatic Water Extraction Index (AWEI) and the self-adaptive Otsu's thresholding method, the second approach is based on the image conversion from RGB (Red-Green-Blue) to HSV (Hue, Saturation, Value) and the use of a parametric threshold, the third approach is based on the use of SAR imagery and an empirically selected threshold. A "static" validation strategy was developed from scratch and standard segmentation metrics were computed to evaluate the accuracy of the three approaches. The average values of the F1 scores on the Sentinel imagery were equal to 0.95, 0.90, and 0.84 for the three approaches, respectively. The same metric on the Landsat imagery was 0.95 for the first approach and 0.93 for the second approach. The best approach, i.e. the AWEI-based method, was then applied to three water bodies in which the effects of the 2022 drought were particularly significant: Sawa lake (Iraq), Poyang lake (China), and Po river (Italy). The results visually highlighted the good performance of the approach in segmenting the water bodies from the surrounding areas.

1. INTRODUCTION

Natural and artificial water reservoirs are essential freshwater resources for human and animal consumption, agricultural irrigation, and several industrial applications. Currently, water level measurements are generally performed by traditional ground instruments such as gauge stations. Indeed, the data collected by these instruments are used to estimate the area and volume of the reservoirs (and their variations over time) using volume-area-elevation curves derived from bathymetric and topographic information of the reservoir itself (Tong et al., 2016, Hamoudzadeh et al., 2023). However, in-situ monitoring is mainly possible in developed countries, due to the difficulties in installing and maintaining measurement stations in remote areas. In addition, even in developed countries, gauge stations are not installed at small and secondary reservoirs. Conversely, the use of Earth Observation (EO) technologies can remarkably reduce the monitoring costs (independent from the actual extent of the reservoir) and provide frequent and regular data that facilitate the continuous monitoring of water reservoirs, in principle with homogeneous worldwide procedures (Valadão et al., 2021).

The aim of this work is precisely included in this background: the general goal is to lay the foundations for the development of a procedure based on free EO data for the routine monitoring of the extent of whichever water reservoir. In particular, in this preliminary analysis focused on multispectral and SAR satellite images, three different segmentation approaches able to distinguish water bodies from the surrounding land surface and measure their extent were investigated using Sentinel-1, Sentinel-2, and Landsat-8 imagery. Indeed, the continuous computation of 2D metrics, such as perimeter and area, is a first step towards the monitoring of the seasonal and annual variations of water reservoirs, allowing the reconstruction of long-term surface water dynamics. This goal is strictly related to the United Nations Sustainable Development Goals (SDGs) concerning water availability (SDG 6 - Clean water and sanitation) and climate change effects monitoring (SDG 13 - Climate action), and to the Recovery Plan Next Generation EU.

2. METHODOLOGY

Three water segmentation approaches were investigated and implemented within Google Earth Engine (GEE). GEE is a cloud computing platform that integrates a wide and freely accessible remote sensing data archive, including Landsat and Sentinel image collections. Through efficient Application Programming Interfaces (APIs), GEE makes it possible to carry out large-scale geospatial analyses, according to the well-known "data-information-knowledge-wisdom" paradigm (Kavvada et al., 2020). In particular, continuing the work started in (Ravanelli et al., 2023), the following three water segmentation approaches were investigated:

- the first (Sengupta et al., 2020, Donchyts et al., 2016) is based on the application of the Automatic Water Extraction Index (AWEI) (Feyisa et al., 2014) and the self-adaptive Otsu's thresholding method (Otsu, 1979) to multispectral imagery;

* Corresponding author

- the second (Valadão et al., 2021) is based on the use of multispectral imagery and the conversion from the RGB (Red-Green-Blue) to the HSV (Hue, Saturation, Value) color model to which a parametric threshold is applied;
- the third (Geohackweek, 2016) is based on the use of SAR imagery and an empirically selected threshold.

The first two approaches were applied to Sentinel-2 (Google Earth Engine Data Catalog, 2023a) and Landsat-8 (Google Earth Engine Data Catalog, 2023c) multispectral imagery, and the third one to Sentinel-1 SAR (Google Earth Engine Data Catalog, 2023b) imagery. For the approaches based on multispectral imagery, only images with a percentage of cloudy pixels less than 30% were selected and a cloud mask was computed to consider only cloud-free pixels using the QA60 bitmask band of Sentinel-2 (Google Earth Engine Data Catalog, 2022) and the QA_PIXEL and QA_RADSAT bands of Landsat-8 (ESA, 2022). For all the approaches, the median reducer was used to aggregate image data over time (Google Earth Engine Documentation, 2023). The median reducer aggregates all the images of an image collection available in a given period and computes an overall median image by calculating the median value of each pixel – for every band – across the temporal stack of images. The median images were the input to the three segmentation approaches. A period of one year was considered in the analyses, in particular, the images collected in 2019 were analysed into three-month sub-periods. In this way, all the images available in 2019 for the three considered satellites were split into four sub-collections to investigate the four seasons separately. Figure 1 and Figure 2 show a median image for Sentinel-2 (after applying the cloud filters) and Sentinel-1 for the period January-March 2019 over the Marghera dock (Venice, Italy), i.e. the validation area, as described in Section 3.

Figure 1. Sentinel-2 multispectral median image (Marghera dock, January-March 2019).

Each approach returned a water segmentation mask as output, from which the area of the reservoir was computed by counting the pixels classified as water and by multiplying the resulting number by the image resolution. Table 1 shows the resolution (pixel size) of the bands used in the analyses.

The following sections describe each approach in detail.

2.1 AWEI approach

In the AWEI-based approach, the water pixels in the input median image were segmented by implementing the AWEI spectral index and by applying the method of local thresholding based on the Otsu's thresholding and the Canny edge detector algorithms (Donchyts et al., 2022). The AWEI index is presented in Equation 1 (Feyisa et al., 2014):

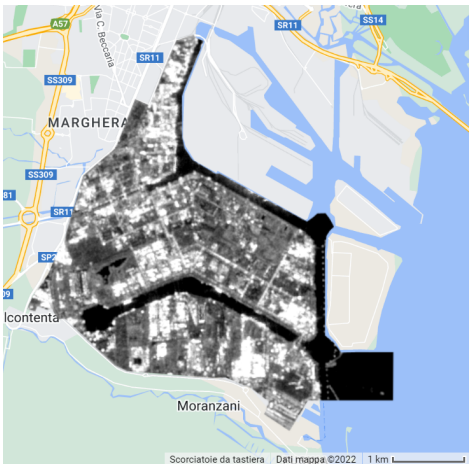

Figure 2. Sentinel-1 median image (Marghera dock, January-March 2019).

Band resolution (pixel size) [m]				
Satellite	RGB	NIR	SWIR1/SWIR2	GRD (IW)
Sentinel-2	10	10	20	-
Landsat-8	30	30	30	-
Sentinel-1	-	-	-	10

Table 1. Band resolution of Sentinel-2, Landsat-8, and Sentinel-1: RGB, Near-infrared (NIR), Short-wave infrared (SWIR), and Ground Range Detected (GRD) Interferometric Wide (IW).

$$AWEI = 4 \cdot (\rho_{GREEN} - \rho_{SWIR1}) - 0.25 \cdot \rho_{NIR} - 2.75 \cdot \rho_{SWIR2} \quad (1)$$

where ρ represents the reflectance for the GREEN (G), SWIR1, SWIR2, and NIR bands, and the coefficients and the arithmetic combinations of the chosen spectral bands were determined by critical examination of the reflectance properties of various land cover types (Feyisa et al., 2014).

The AWEI index allows for maximization of the separability of water and non-water pixels and thereby makes it possible to extract surface water with high accuracy (Feyisa et al., 2014). Unlike the Normalized Difference Water Index (NDWI) or the Modified Normalized Difference Water Index (MNDWI), the use of AWEI index avoids segmentation errors due to many factors such as clouds, snow, and ice. Additionally, the AWEI does not commit errors of commission (false positive segmentation of water) in areas with shadows due to topographic conditions or the presence of cloud shadows (Donchyts et al., 2016). The increase in the contrast between water and other dark surfaces provided by this index compared to the NDWI index is shown in Figure 3.

After the AWEI index computation, the method of local thresholding based on Otsu's thresholding, and the Canny edge detector algorithm were applied to reduce the number of input pixels only to those located near water-land edges (Donchyts et al., 2016). The detection of water pixels was then refined using morphological dilation. Figure 4 shows the water mask generated using the approach applied to Sentinel-2 imagery.

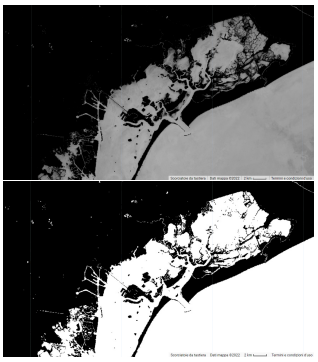

Figure 3. Comparison between NDWI (above) and AWEI (below) resulting images on the same area (Venice lagoon).

Figure 4. Water segmentation image obtained with the AWEI approach using Sentinel imagery.

2.2 HSV approach

In the HSV-based approach (Valadão et al., 2021), the input median RGB image (see Figure 1) was firstly transformed to HSV. Only the Hue band was selected to facilitate the subsequent identification of the water pixels (Valadão et al., 2021). In this case, the water segmentation was based on a parametric threshold: more specifically, only the pixels in the 0.25-0.95 tonality range were classified as water pixels. The resulting water segmentation mask is shown in Figure 5.

2.3 SAR approach

The Sentinel-1 images were filtered by selecting only the VV polarisation. It is important to underline two issues that affect SAR imagery. Firstly, some surfaces alter the polarisation of the SAR signal, but this is usually not frequent for water body segmentation. Secondly, SAR images are often affected by speckle noise that deteriorates the quality of the image (Geohackweek, 2016). To reduce the speckle, a focal median filter was applied. Then, a simple threshold method was implemented to identify water pixels in the SAR images. Specifically, a threshold of backscatter was chosen and all pixels below that threshold were classified as water. The selected threshold value was -16 dB and it was empirically selected by visually inspecting the histogram representing the number of pixels and the intensity of the backscattered signal (Figure 6).

The water segmentation mask obtained with this approach is shown in Figure 7.

Figure 5. Water segmentation image obtained with the HSV approach using Sentinel imagery.

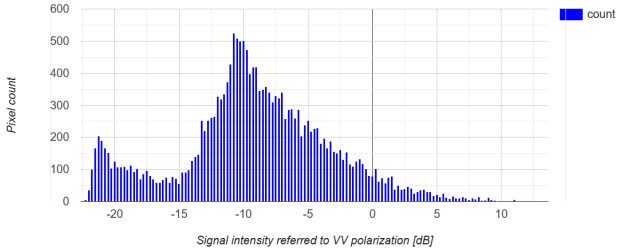

Figure 6. Histogram for SAR threshold selection.

Figure 7. Water segmentation image obtained with the SAR approach using Sentinel imagery.

3. VALIDATION

The three approaches were validated using a “static” validation strategy, i.e, considering a validation area where the water level variations do not impact the water surface extent over time and the geometry of the water borderlines is available as an independent ground truth. Specifically, the different approaches were applied to the harbour area of Marghera considering the 2019 year and the results were compared with the reference shapefile of the Site of National Interest (SIN) of Marghera available on the Ministry of Environment and Energy Secur-

ity website of the Italian Government. In the selected area, the water borderlines are artificial and, therefore, in theory, independent from the water level, allowing to compare the performances of the three approaches using imagery acquired in different epochs. The reference ground truth and the generated water masks are shown in Figure 8.

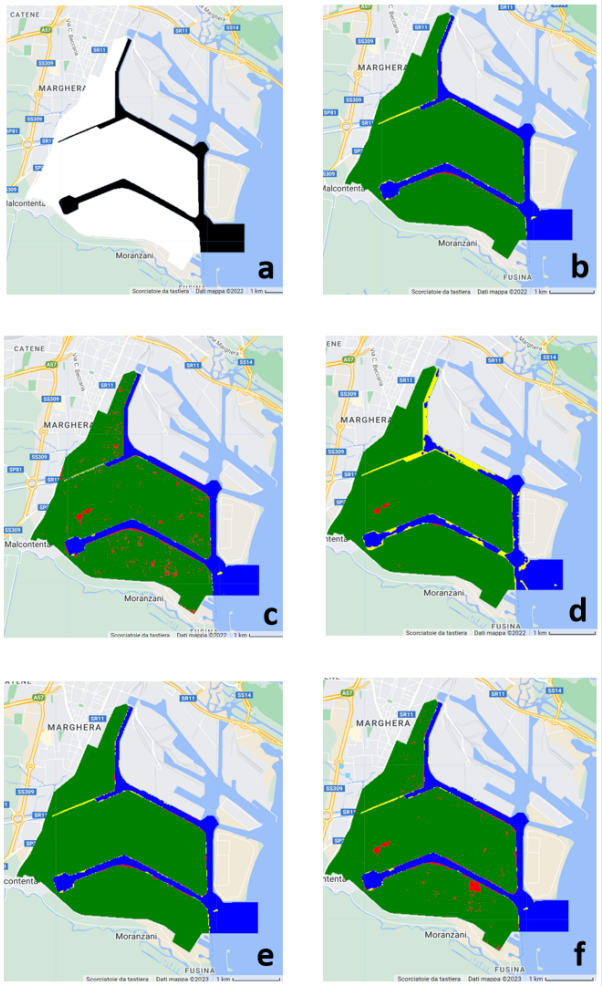

Figure 8. Ground truth mask (a) and water detection masks obtained with the first approach on Sentinel imagery (b) and Landsat imagery (e), the second approach on Sentinel imagery (c) and Landsat imagery (f), and the third approach (d) (Marghera dock, January-March 2019). True positives are in blue, true negatives in green, false positives in red and false negatives in yellow.

Figure 8-b and 8-e visually demonstrate how the AWEI approach performs better than the other ones. Figure 8-c shows that the HSV approach generates a higher number of false positive pixels compared to the AWEI approach. Moreover, the HSV approach not only fails to segment the pixels of land located on the water-land border but also those located inland. The reason is related to the presence of a few roofs in the validation area: their color falls in the Hue range of 0.25-0.95, which was set to classify water in this approach. To further improve the performance of this method, a solution could be to narrow down the Hue range or select a non-urban validation area. Figure 8-d highlights that the SAR approach presents many segmentation issues and provides the worst results. In this case, the number of pixels segmented as false negatives is higher, i.e. a lot of water pixels are segmented as land pixels. Finally, by analyzing Figure 8-d it is possible to notice that the small portion in the hinterland classified as false positive is actually an area where the algorithm works correctly and the reference is not correct. That area is indeed a small wet area that in the reference image was mistakenly considered land. This affects also the second method.

For each approach, the confusion matrix was computed using both Sentinel and Landsat collections to investigate the performance of the investigated approaches. The following standard metrics were computed: Accuracy (A), Intersection over Union (IoU), Precision (P), Recall (R), and F1 score (F1). The results are presented in Tables 2, 3, 4, 5, and 6.

Temporal range	Images	A	IoU	P	R	F1
Q1 2019	12	0.98	0.92	0.97	0.94	0.96
Q2 2019	7	0.98	0.90	0.99	0.91	0.95
Q3 2019	9	0.98	0.91	0.99	0.92	0.95
Q4 2019	8	0.98	0.89	0.95	0.94	0.94

Table 2. Metrics of the AWEI approach with a time range of three months (Sentinel-2).

Temporal range	Images	A	IoU	P	R	F1
Q1 2019	15	0.98	0.92	0.98	0.94	0.96
Q2 2019	13	0.98	0.90	0.97	0.93	0.95
Q3 2019	17	0.98	0.91	0.98	0.93	0.95
Q4 2019	10	0.98	0.89	0.95	0.94	0.94

Table 3. Metrics of the AWEI approach with a time range of three months (Landsat-8).

Temporal range	Images	A	IoU	P	R	F1
Q1 2019	12	0.97	0.86	0.86	0.97	0.92
Q2 2019	7	0.97	0.84	0.86	0.96	0.91
Q3 2019	9	0.96	0.82	0.85	0.97	0.90
Q4 2019	8	0.95	0.78	0.79	0.97	0.87

Table 4. Metrics of the HSV approach with a time range of three months (Sentinel-2).

Temporal range	Images	A	IoU	P	R	F1
Q1 2019	15	0.97	0.87	0.91	0.96	0.93
Q2 2019	13	0.98	0.88	0.95	0.93	0.94
Q3 2019	17	0.98	0.89	0.95	0.93	0.94
Q4 2019	10	0.97	0.84	0.87	0.95	0.91

Table 5. Metrics of HSV approach with a time range of three months (Landsat-8).

Temporal range	Images	A	IoU	P	R	F1
Q1 2019	44	0.95	0.73	0.98	0.74	0.84
Q2 2019	46	0.95	0.71	0.98	0.72	0.83
Q3 2019	47	0.95	0.72	0.98	0.73	0.84
Q4 2019	44	0.95	0.73	0.98	0.73	0.84

Table 6. Metrics of the SAR approach with a time range of three months (Sentinel-1).

Again, Tables 2, 4 and 6 demonstrate that the first approach performs better than the others: all the metrics, except the Recall, are higher than the corresponding ones of the other approaches. In particular, the average F1 scores of the three approaches applied to Sentinel-2 (first and second approach) and Sentinel-1 (third approach) imagery are equal to 0.95, 0.90, and 0.84, respectively. The same metric values on the Landsat imagery are 0.95 for the first approach and 0.93 for the second one. Furthermore, by comparing changes in F1 scores through the subperiods for each approach in Tables 2, 4 and 6, it is possible to notice that the AWEI and SAR methods are less affected by seasonality compared to the HSV method. This behaviour can be related to the different lighting conditions in the median images during winter and summer. The HSV method segments

water pixels based on a Hue range: variations in the lightness conditions cause a change in Hue conditions, and therefore affect the performance of this approach. The differences between the seasons can be visually appreciated in Figure 9, in which black areas highlight the pixels that are misclassified as false positives for the summer (right) period while they are correctly classified in the winter period (left).

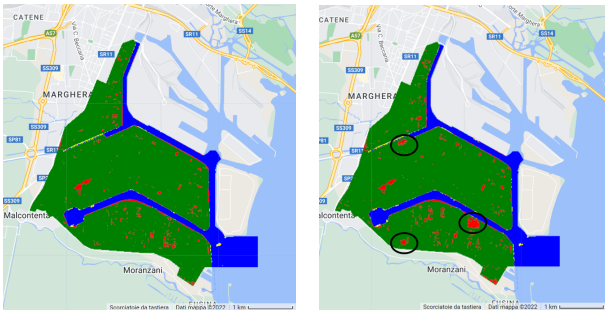

Figure 9. Results comparison between January-March 2019 (left) and July-September 2019 (right) for the second approach.

Finally, Table 6 highlights that the number of SAR images available for each period is higher than the number of multispectral images. This is related to two reasons: firstly the area of Marghera is located at the intersection of several orbits of the Sentinel-1 satellite, both ascending and descending; secondly, SAR images are not affected by clouds, therefore no cloud filter was applied to remove images.

4. CASE STUDIES

The best method (i.e. the AWEI approach) was applied to three case studies in which the effects of the 2022 drought were particularly significant. For sake of brevity, only the results obtained using Sentinel-2 images are shown below.

4.1 Sawa Lake

Sawa Lake is an endorheic lake (4.5 km long and 1.8 km wide) located in southern Iraq in the governorate of Muthanna, near the Euphrates River. The water level in the lake used to fluctuate between dry and wet seasons, but despite being situated in an arid region, in 2022 it did not dry up because of the balance between evaporation and water feed, i.e. based on rainfall and groundwater through cracks and fissure (Service, 2015). Sawa Lake was severely affected by the 2022 water crisis caused by climate change, which led to low rainfall and drought, but also by lack of maintenance of water infrastructure and by the presence of dams in upstream countries that reduced the flow of the Tigris and Euphrates rivers (Radeef and Abdulameer, 2023). Lake Sawa degradation started more than 10 years ago, but in 2022 the lake disappeared for the first time (Copernicus, 2022). This effect can be appreciated in Figure 10 by comparing the median image obtained for the period January-March 2020 with the corresponding one of 2022.

The application of the AWEI-based method to this lake returned the water masks shown in Figure 11.

The water area was obtained from these masks to quantify the change: the area decreased from 3.90 km^2 in 2020 to 0.39 km^2 in 2022.

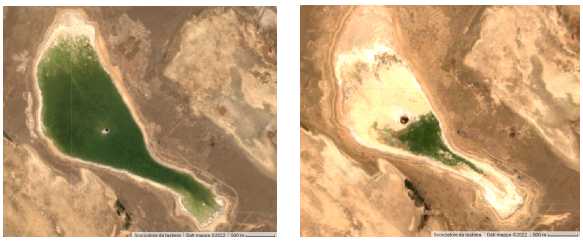

Figure 10. Sentinel-2 median image of Sawa lake on January-March 2020 (left) and on January-March 2022 (right).

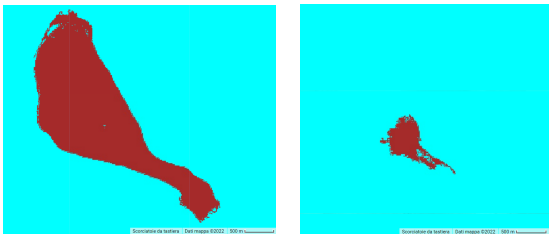

Figure 11. Water detection image on January-March 2020 (left) and January-March 2022 (right).

4.2 Poyang Lake

Poyang Lake is located in Jiujiang, in China’s Jiangxi Province and it is the largest freshwater lake in China. The lake is fed by the Gan, Xin, and Xiu rivers which connect to the Yangtze through a narrow channel. Poyang Lake routinely fluctuates in size between the winter and summer seasons: in winter, water levels on the lake are typically low, then summer rains cause it to swell. However, in recent years, the size of the lake has been decreasing overall. In particular, during the summer of 2022, the Yangtze River basin was affected by a prolonged heat wave and drought, and therefore Poyang Lake dried up reaching water levels not seen in decades. On June 23, the Xingzi Station measured the highest water levels of the year on Poyang Lake; after that, the Jiangxi Hydrological Monitoring Center recorded high temperatures and a lack of rain, i.e. the factors that caused the lake to drop rapidly (NASA, 2022). On August 6, water levels had declined to 11.99 meters and the Center identified this date as the start of the lake dry season: water levels have continued to drop, registering 8.96 meters on August 30. In this case, the comparison was made between Spring 2022 (i.e. median image obtained for the period April-June 2022) and Summer 2022 (i.e. median image obtained for the period July-September 2022). The median images depicted in Figure 12 show this trend, and the measures of the areas confirm it: from the masks represented in Figure 13, areas of 2281.48 km^2 and 1054.61 km^2 were obtained for Spring 2022 and for Summer 2022, respectively.

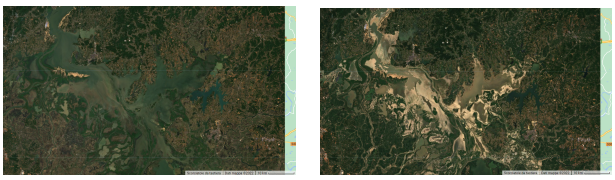

Figure 12. Sentinel-2 median image of Poyang lake on April-June 2022 (left) and on July-September 2022 (right).

4.3 Po river

Po river is the longest river in Italy (652 km). It is located in the North of Italy and flows from east to west crossing many im-

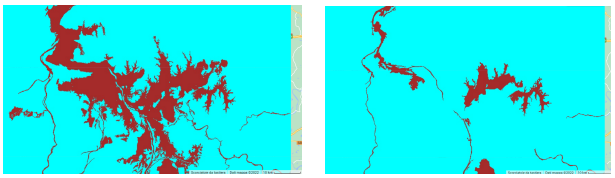

Figure 13. Water detection image on April-June 2022 (left) and on July-September 2022 (right).

portant Italian cities. The vast valley around the Po is called the Po Basin: about 20 million people live there (a third of the Italian population) and it is the main industrial area and the largest agricultural area in the country, accounting for 35% of Italian agricultural production (Borzì et al., 2021). Moreover, the water of the Po river is essential for the energy production of the country. Its flow is controlled by lots of dams that work as hydroelectric power plants and there are several thermoelectric power stations that use the water of the Po basin as coolant. During 2022, due to the intense drought, the water level of the river reached a historic low in the principal sections and the flow touched its all-time low (Po River Basin District Authority, 2022). The analysis was carried out by comparing Spring 2020 and Spring 2022 in a 50 km portion of the Po river near Piacenza. The results are shown in Figure 14 and 15, where it is possible to observe a reduction of the surface from 14.72 km^2 to 11.22 km^2, i.e. about 25% in only two years.

Figure 14. Sentinel-2 median image of Po river on April-June 2020 (above) and on April-June 2022 (below).

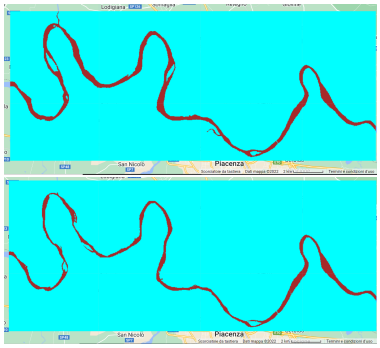

Figure 15. Water detection image on April-June 2020 (above) and on April-June 2022 (below).

5. CONCLUSIONS AND FUTURE PERSPECTIVES

The aim of this work was to lay the foundations for the development of a methodology for the continuous monitoring of water reservoirs through the analysis of multispectral and SAR satellite images. The main objective was to implement a segmentation strategy able to distinguish water from the surrounding land surface and then to measure the planimetric extent of water reservoirs starting from the area occupied by the water pixels identified in the retrieved masks. In particular, three different approaches were implemented within GEE and applied to Sentinel-1, Sentinel-2 and Landsat-8 imagery. The first approach is based on the use of the AWEI and the self-adaptive Otsu’s thresholding method; the second approach is based on the image conversion from RGB to HSV and the use of a parametric threshold; the third approach is based on the use of SAR imagery and an empirically selected threshold. A “static” validation strategy was developed from scratch and standard segmentation metrics were computed to evaluate the accuracy of the three approaches. The average values of the F1 scores on the Sentinel imagery were equal to 0.95, 0.90 and 0.84 for the three approaches, respectively. The same metric on the Landsat imagery was 0.95 for the first approach and 0.93 for the second approach. The best approach (the AWEI-based method) was then applied to three water bodies in which the effects of the 2022 drought were particularly significant: Sawa lake (Iraq), Poyang lake (China), and Po river (Italy). The results visually highlighted the good performance of the approach in segmenting the water bodies from the surrounding areas.

Nevertheless, an adequate monitoring of water reservoirs includes not only the estimation of the extent of their surface but also the quantification of their volume. This paper focused on the extent estimation since the continuous computation of 2D metrics is a first step towards the monitoring of the seasonal and annual variations of water reservoirs, allowing the reconstruction of long-term surface water dynamics.

As for future developments, the validation will be extended to other areas. In this work, the validation was carried out on the SIN of Marghera dock, and this choice introduced additional errors in the validation itself due to the presence of nearby buildings and vegetation. Moreover, the dock area was selected because in this area the water surface remains constant over time. The generation of a dataset starting from high-resolution satellite images will allow validation of the methodology on dynamic references too, increasing the generalization of the methodology. Furthermore, the generation of the dataset may lead the way to the development and testing of data-driven approaches, such as deep learning algorithms. Regarding the SAR results, future development will investigate a threshold selection method based on automatic approaches (e.g. Otsu’s thresholding), instead of parametric thresholds. Finally, the combination of the three tested approaches will be investigated to improve the results.

ACKNOWLEDGEMENTS

This project has received funding from the European High-Performance Computing Joint Undertaking (JU) under grant agreement No 951745. The JU receives support from the European Union’s Horizon 2020 research and innovation programme and Germany, Italy, Slovenia, France, Spain.

REFERENCES

Borzì, I., Monteleone, B., Bonaccorso, B., Martina, M., 2021. Estimating the economic impacts of drought on agriculture through models and surveys in the Po river basin (Northern Italy). *EGU General Assembly Conference Abstracts*, EGU21–12066.

Copernicus, 2022. Al Sawa Lake has completely dried up — Copernicus — copernicus.eu. www.copernicus.eu/en/media/image-day-gallery/al-sawa-lake-has-completely-dried. [Accessed 08-Feb-2023].

Donchyts, G., Schellekens, J., Winsemius, H., Eisemann, E., Van de Giesen, N., 2016. A 30 m resolution surface water mask including estimation of positional and thematic differences using landsat 8, srtm and openstreetmap: a case study in the Murray-Darling Basin, Australia. *Remote Sensing*, 8(5), 386.

Donchyts, G., Winsemius, H., Baart, F., Dahm, R., Schellekens, J., Gorelick, N., Iceland, C., Schmeier, S., 2022. High-resolution surface water dynamics in Earth's small and medium-sized reservoirs. *Scientific reports*, 12(1), 1–13.

ESA, 2022. Cloud Masks. https://sentinel.esa.int/web/sentinel/technical-guides/sentinel-2-msi/level-1c/cloud-masks.

Feyisa, G. L., Meilby, H., Fensholt, R., Proud, S. R., 2014. Automated Water Extraction Index: A new technique for surface water mapping using Landsat imagery. *Remote Sensing of Environment*, 140, 23–35.

Geohackweek, 2016. SAR water body classification. https://mbonnema.github.io/GoogleEarthEngine/07-SAR-Water-Classification/.

Google Earth Engine Data Catalog, 2022. Sentinel-2 MSI: MultiSpectral Instrument, Level-2A. https://developers.google.com/earth-engine/datasets/catalog/COPERNICUS_S2_SR. [Accessed 28-Feb-2023].

Google Earth Engine Data Catalog, 2023a. Harmonized Sentinel-2 MSI: MultiSpectral Instrument, Level-2A — developers.google.com. https://developers.google.com/earth-engine/datasets/catalog/COPERNICUS_S2_SR_HARMONIZED. [Accessed 28-Feb-2023].

Google Earth Engine Data Catalog, 2023b. Sentinel-1 SAR GRD: C-band Synthetic Aperture Radar Ground Range Detected, log scaling — developers.google.com. https://developers.google.com/earth-engine/datasets/catalog/COPERNICUS_S1_GRD. [Accessed 28-Feb-2023].

Google Earth Engine Data Catalog, 2023c. USGS Landsat 8 Level 2, Collection 2, Tier 1 — developers.google.com. https://developers.google.com/earth-engine/datasets/catalog/LANDSAT_LC08_C02_T1_L2#description. [Accessed 28-Feb-2023].

Google Earth Engine Documentation, 2023. Reducer Overview. https://developers.google.com/earth-engine/guides/reducers_intro. Online; accessed February, 2023.

Hamoudzadeh, A., Ravanelli, R., Crespi, M., 2023. GEDI data within Google Earth Engine: preliminary analysis of a resource for inland surface water monitoring. *The International Archives of the Photogrammetry, Remote Sensing and Spatial Information Sciences*. In press.

Kavvada, A., Metternicht, G., Kerblat, F., Mudau, N., Haldorson, M., Laldaparsad, S., Friedl, L., Held, A., Chuvieco, E., 2020. Towards delivering on the Sustainable Development Goals using Earth observations. *Remote Sensing of Environment*, 247.

NASA, 2022. Parched Poyang Lake — earthobservatory.nasa.gov. https://earthobservatory.nasa.gov/images/150285/parched-poyang-lake. [Accessed 09-Feb-2023].

Otsu, N., 1979. A Threshold Selection Method from Gray-Level Histograms. *IEEE Transactions on Systems, Man, and Cybernetics*, 9(1), 62-66.

Po River Basin District Authority, 2022. Report of 22 July 2022 - Po River. *Permanent observatory on water uses in the hydrographic district of the river Po*.

Radeef, H. A., Abdulameer, I. M.-A., 2023. The Water Area of Sawa Lake as Derived from Land Surface Temperature and Remote Sensing Data. *Ibn AL-Haitham Journal For Pure and Applied Sciences*, 36(1), 100–112. https://doi.org/10.30526/36.1.2873.

Ravanelli, R., Mazzucchelli, P., Belloni, V., Bocchino, F., Morselli, L., Fiorino, A., Gerace, F., Crespi, M., 2023. Earth Observation Big Data exploitation for water reservoirs continuous monitoring: the potential of Sentinel-2 data and HPC. C. Ieracitano, N. Mammone, M. Di Clemente, M. Mahmud, R. Furfaro, F. C. Morabito (eds), *The Use of Artificial Intelligence for Space Applications: Workshop at the 2022 International Conference on Applied Intelligence and Informatics*, Studies in Computational Intelligence. In press.

Sengupta, D., Chen, R., Meadows, M. E., Banerjee, A., 2020. Gaining or losing ground? Tracking Asia's hunger for 'new' coastal land in the era of sea level rise. *Science of The Total Environment*, 732, 139290.

Service, R. S. I., 2015. Sawa Lake — Ramsar Sites Information Service — rsis.ramsar.org. https://rsis.ramsar.org/ris/2240. [Accessed 28-Feb-2023].

Tong, X., Pan, H., Xie, H., Xu, X., Li, F., Chen, L., Luo, X., Liu, S., Chen, P., Jin, Y., 2016. Estimating water volume variations in Lake Victoria over the past 22years using multi-mission altimetry and remotely sensed images. *Remote Sensing of Environment*, 187, 400-413.

Valadão, L. V., Cicerelli, R. E., de Almeida, T., Ma, J. B. C., Garnier, J., 2021. Reservoir metrics estimated by remote sensors based on the Google Earth Engine platform. *Remote Sensing Applications: Society and Environment*, 24(100652).